ASSESSMENT OF THE PERFORMANCE OF AN ANOXIC-AEROBIC MICROALGAL-BACTERIAL SYSTEM TREATING DIGESTATE

Andrés F. Torres-Franco [a, b, c], Maribel Zuluaga [a, b, d], Diana Hernández-Roldán [a, b, d], Deborah Leroy-Freitas [a, b, c], Cristian A. Sepúlveda-Muñoz [a, b], Saúl Blanco [e, f], César R. Mota [c], Raúl Muñoz [a, b *]

[a] Department of Chemical Engineering and Environmental Technology, Valladolid University, Dr. Mergelina, s/n., 47011 Valladolid, Spain.

[b] Institute of Sustainable Processes, Dr. Mergelina, s/n, 47011, Valladolid, Spain.

[c] Department of Sanitary and Environmental Engineering, Federal University of Minas Gerais, Belo Horizonte, 31270-010, Brazil.

[d] Faculty of Environmental Engineering UPAEP University, Puebla, 21 Sur 1103, Barrio de Santiago, 72410, Puebla, México.

[e] University of León, Campus de Vegazana, 24071, León, Spain.

[f] Laboratory of Diatomology. Institute of Environment, Natural Resources and Biodiversity. La Serna 58, 24007, León, Spain

* Corresponding author: mutora@iq.uva.es, *Tel*: (34) 983-186-424 (R. Muñoz)

Abstract

The performance of an anoxic-aerobic microalgal-bacterial system treating synthetic food waste digestate at 10 days of hydraulic retention time via nitrification-denitrification under increasing digestate concentrations of 25%, 50%, and 100%(v/v) was assessed during Stages I, II and III, respectively. The system supported adequate treatment without external CO_2 supplementation since sufficient inorganic carbon in the digestate was available for autotrophic growth. High steady-state Total Organic Carbon (TOC) and Total Nitrogen (TN) removal efficiencies of 85-96% and 73-84% were achieved in Stages I and II. Similarly, PO_4^{3-}-P removals of 81±15% and 58±4% were recorded during these stages. During Stage III, the average influent concentrations of 815±35 mg TOC·L^{-1}, 610±23 mg TN·L^{-1}, and 46±11 mg PO_4^{3-}-P·L^{-1} induced O_2 limiting conditions, resulting in TOC, TN and PO_4^{3-}-P removals of 85±3%, 73±3%, and 28±16%, respectively. Digestate concentrations of 25% and 50% favored nitrification-denitrification mechanisms, whereas the treatment of undiluted digestate resulted in higher ammonia volatilization and hampered nitrification-denitrification. In Stages I and II, the microalgal community was dominated by *Chlorella vulgaris* and *Cryptomonas* sp., whereas *Pseudoanabaena* sp. was more abundant during Stage III. Illumina sequencing revealed the presence of carbon and nitrogen transforming bacteria, with dominances of the genera *Gemmata*, *Azospirillum,* and *Psychrobacter* during Stage I, II, and III, respectively. Finally, the high settleability of the biomass (98% of suspended solids removal in the settler) and average C (42%), N (7%), P (0.2%), and S (0.4%) contents recovered in the biomass confirmed its potential for agricultural applications, contributing to a closed-cycle management of food waste.

Keywords: microalgal-bacterial symbiosis, digestate, nitrification-denitrification, microalgae, photobioreactor.

1 Introduction

High-strength wastewaters, such as livestock effluents or anaerobic digestates, present high concentrations of nitrogen (mainly in the form of ammonia) and phosphorous, representing a challenge to both natural ecosystems and to conventional wastewater treatment technologies. However, this high nutrient load also represents an opportunity for the simultaneous recovery of these nutrients and the production of added-value bioproducts (Makádi et al., 2012). Many physical/chemical wastewater treatment technologies, such as ammonia stripping, phosphate adsorption or nutrient precipitation, have been investigated with promising results, but they exhibit high energy and chemical demands, and reduced environmental sustainability (Rehl & Müller, 2011; Yuan et al., 2016; Rahman et al., 2019). In this context, microalgae-based systems have gained increasing attention in the past decade as an alternative platform for the sustainable treatment of high-strength wastewaters due to their potential to efficiently remove and recover carbon and nutrients, while producing valuable microalgal biomass with multiple applications. The most popular valorization strategies of microalgae biomass include the production of biofuels, biogas, animal feed, biofertilizers, and biostimulants (Stiles et al., 2018).

Among the different microalgae-based treatments investigated in recent years, anoxic-aerobic microalgal-bacterial systems have emerged as a highly efficient alternative for the removal of nutrients from wastewaters with a low carbon to nutrient ratio (de Godos et al., 2014; Alcántara et al., 2015a; García et al., 2017a; Dhaouefi et al., 2018). The main mechanisms underlying the removal of nitrogen in these systems are nitrification-denitrification and assimilation in the form of microbial protein (de Godos et al., 2014; Dhaouefi et al., 2018). The nitrification-denitrification process is based on the initial aerobic transformation of ammonia nitrogen into nitrite (NO_2) and nitrate (NO_3) by nitrifiers, followed by the reduction of these oxidized nitrogen compounds into

63 N_2 by denitrifying microorganisms using biodegradable organic matter as the electron donor.
64 Nitrification-denitrification and nitrogen assimilation are more sustainable alternatives for the
65 removal of nitrogen in microalgae-based treatments than free ammonia (NH_3) volatilization, since
66 N_2 is an inert gas with no environmental impact in the atmosphere, whereas NH_3 is a greenhouse
67 gas precursor (Alcántara et al., 2015b). The oxygen demand for nitrification in microalgae-bacteria
68 systems is supplied by in-situ photosynthetic aeration (Galès et al., 2019). In the anoxic-aerobic
69 configuration, photo-aeration, microalgae growth (with concomitant assimilation of nitrogen and
70 phosphorus, Eq. 1) and nitrification (Eq. 2), take place in the photobioreactor, from which
71 nitrate/nitrite are recycled for their reduction to N_2 via denitrification (Eq. 3) to an anoxic tank.
72 The anoxic tank is also fed with the influent wastewater and the biomass recirculated from the
73 settler (De Godos et al., 2014).

74 $$2H_2O + CO_2 + hv + NH_4^+ + PO_4^{3-} \rightarrow CH_2ONP\ (microalgae) + 2O_2 + 4H_2O \quad (1)$$

75 $$NH_4^+ + 2N_2 \rightarrow NO_3^- + 2H^+ + H_2O \quad (2)$$

76 $$8NO_3^- + 5CH_3COOH \rightarrow 8HCO_3^- + 6H_2O + 2CO_2 + 4N_2 \quad (3)$$

77 This innovative configuration has been successfully tested during the treatment of domestic and
78 textile wastewater. For instance, García et al. (2017a) reported carbon and nitrogen removal
79 efficiencies of 90±2% and 81±3%, respectively, during the treatment of real domestic wastewater
80 at 2 days of hydraulic retention time (HRT), with the addition of external CO_2 and pH control in
81 the aerobic photobioreactor. Similarly, Dhaouefi et al. (2018) recorded nitrogen removal
82 efficiencies of 87±11% during textile wastewater treatment at 10 days of HRT. However, the
83 potential of this technology for digestate treatment needs to be explored further. The high ammonia
84 loads typically present in digestates may not be completely nitrified in anoxic-aerobic
85 photobioreactors due to limited photo-aeration, which may result in high free ammonia

concentrations in the reactors limiting microalgae and nitrifiers activity (Collos & Harrison, 2014; Gutiérrez et al., 2016).

This study assessed the influence of digestate loading rate on carbon and nutrient removal in an anoxic-aerobic microalgae-bacteria system engineered with biomass settling and recirculation and without external CO_2 supplementation. The novelty of this work relies on the assessment of the performance of this novel photobioreactor configuration for the treatment of high carbon and nitrogen loads of up to 6-fold the influent loads reported in previous experiences (*e.g.,* García et al., 2017; Toledo-Cervantes et al., 2019), under the hypothesis that high removal efficiencies will be achieved at these high loading conditions. The mechanisms underlying C, N, and P removal and recovery in the anoxic tank and open photobioreactor treating synthetic food waste digestate (SFWD) were assessed using a mass balance approach. A detailed characterization of the dynamics of microalgal and bacterial population structure was conducted using morphological and molecular identification tools. Finally, the valorization potential of the microalgal-bacterial biomass was discussed based on the characterization of nutrients recovered in this biomass.

2 Material and Methods

2.1 Synthetic food waste digestate composition

Synthetic food waste digestate (SFWD) was used in this study as a model of high-strength wastewater. The SFWD was modified from Frutos et al (2016), based on data from real food digesters operated at the National Institute of Science and Technology for Sustainable Wastewater Treatment (Brazil), and prepared with a composition of (per liter of tap water): 850 mg $C_8H_5KO_4$, 400 mg meat extract, 330 mg casein peptone, 100 mg urea, 1700 mg NH_4Cl, 300 mg KH_2PO_4 ·

$3H_4O$, 18 mg NaCl, 10 mg $CaCl_2$, 5 mg $MgSO_4$ and 5000 mg $NaHCO_3$. This composition resulted in concentrations of dissolved total organic carbon (TOC) of 840 mg L^{-1}, a chemical oxygen demand (COD) of 2530 mg L^{-1}, 650 mg L^{-1} of dissolved inorganic carbon (IC), and 710 mg L^{-1} of total nitrogen (TN). The SFWD corresponded to a liquid fraction of digestate with a low content of easily biodegradable carbon and a low C:N ratio (1:1 to 4:1, based on COD and TN). The SFWD was freshly prepared twice a week and stored at 4 °C prior to be fed to the system with a peristaltic pump (Watson Marlon 313D, UK).

2.2 Experimental set-up

The experimental set-up consisted of an anoxic-aerobic microalgal-bacterial system with the configuration showed in Figure 1. The working volumes of the anoxic tank (*Ax*), open photobioreactor (*OPBR*) and settler were 2.85 L, 9.15 L and 1 L, respectively. The inoculum used in the experimental set-up, obtained from a microalgal-bacterial culture treating municipal wastewater, was dominated by *Chlorella vulgaris*, *Nitzschia* sp., *Pseudoanabaena* sp., and *Tetradesmus obliquus*. The *OPBR* exhibited an illuminated area of 0.045 m^2, with lighting supplied for 12 h per day by white LED lamps (Phillips) located above the pond, which provided an average light intensity of 1314±12 μmol m^2 s^{-1} at the culture broth surface (Toledo-Cervantes et al., 2019), simulating outdoor conditions. The *Ax* consisted of an air-tight tank. Submerged pumps (Eheim CompactON 300, Germany) provided complete mixing in the cultivation broth of *Ax* and *OPBR*. Peristaltic pumps (Masterflex, Cole Parmer, UK) were used to continuously recirculate the microalgae-bacteria biomass from the bottom of the conical secondary settler to *Ax* and from *OPBR* to *Ax* at flowrates of 0.6 L d^{-1} (external) and 2.4 L d^{-1} (internal recycling), respectively.

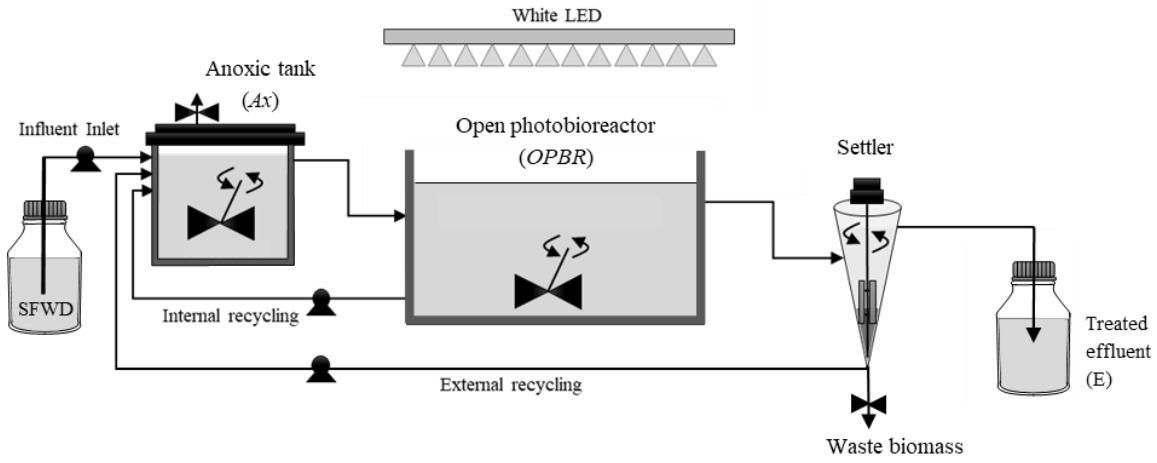

Figure 1. Schematic diagram of the anoxic-aerobic microalgae-bacteria photobioreactor set-up.

2.3 Experimental design

The microalgal-bacterial anoxic-aerobic system was operated continuously at an HRT of 10 d (corresponding to an influent SFWD flow rate of 1.2 L d^{-1}) and a temperature of 27±2 ℃. Biomass was wasted from the bottom of the secondary settler in order to maintain the solids retention time (SRT) at 18 d. A high SRT was selected to favor the acclimation of microalgae and bacteria to the high strength of the SFWD and prevent the wash-out of nitrifiers. The experimental set-up was operated for 138 d under step increases in SFWD load in order to assess the capacity of the anoxic-aerobic system to support a sequential nitrification of the influent NH_4^+ and the further reduction into N_2 of the NO_2^- and NO_3^- produced in the *OPBR* (De Godos et al., 2014). The experiment was divided into three operational stages. During the first 40 days (Stage I, S-I), the anoxic-aerobic system was fed with 25% (v/v) diluted SFWD. SFWD load was increased to 50% from days 41 to 87 (Stage II, S-II) and finally increased to 100% during the last stage of operation from day 89 to 138 (Stage III, S-III).

Liquid samples of 100 mL from the SFWD, *Ax*, *OPBR*, settled biomass, and effluent were collected twice a week and filtered through 0.20 μm nylon filters (Fisherbrand™, Fisher Scientific, UK) to

145 determine the concentrations of TOC, IC, TN, NH_4^+-N, NO_2^--N, NO_3^--N, PO_4^{3-}-P, TSS, and VSS. The
146 ambient and cultivation broth temperatures, influent and recycling flow rates, dissolved oxygen
147 (DO) concentration and pH, were measured daily in the system. During steady-state at each
148 operational stage, samples for the determination of total phosphorus (TP) and COD from the
149 anoxic-aerobic system were drawn in triplicate, along with samples of waste biomass for the
150 analyses of the C, N, and P content of the microalgae-bacteria biomass. Samples of 2 mL for
151 identification and quantification of microalgae populations were collected from the *OPBR* at the
152 end of each steady-state and preserved in 5% lugol and 10% formaldehyde and stored at 4 °C prior
153 to analysis. Additionally, biomass samples from the *OPBR* were harvested at the end of each
154 steady-state and frozen-stored at -4 °C in order to evaluate the richness and composition of the
155 bacterial communities.

156 **2.4 Analytical procedures**

157 The concentrations of TSS, VSS, TP, and COD were determined according to standard methods
158 (2012). The DO concentration and temperature were monitored with an OXI 330i oximeter (WTW,
159 Germany), while a pH meter Eutech Cyberscan pH 510 (Eutech Instruments, The Netherlands)
160 was used for pH determination. A Shimadzu TOC-VCSH analyzer (Shimadzu, Japan) connected
161 to a TNM-1 module was used for the determination of the concentrations of TOC, IC, and TN. The
162 concentrations of NH_4^+-N were determined using an Orion Dual Star electrode (ThermoScientific,
163 The Netherlands). The fraction of free ammonia (FAN) was estimated on the basis of the NH_4^+-N
164 concentrations and pH ($FAN = NH_4^+(1 + 10^{pK_a - pH})^{-1}$). The analyses of the C and N biomass
165 content were carried out using a FLASH 2000 Elemental Analyzer (ThermoScientific, The
166 Netherlands) with pre-dried and grinded microalgae-bacteria biomass. The content of P in the

biomass was measured using a 725-ICP Optical Emission Spectrophotometer (Agilent, USA). The quantification, identification, and biometry measurements of microalgae population structure were carried out by microscopic examination of the samples fixed in lugol and formaldehyde using an inverted microscope (OLYMPUS IX70, USA). Cell quantification was performed using the Utermöhl technique (Sournia, 1978), and final microalgae densities and biometry measurements for each species were reported as the averaged results from fixed samples.

2.5 Mass balance calculations

Mass balances in *Ax* and *OPBR* were performed for TOC, IC, TN, NH_4^+-N and PO_4^{3-}-P, considering the flowrates and concentrations of the target parameters in the SFWD feed, effluent, and biomass wastage. The global removal efficiencies ($RE_{i,Ax-OPBR}$) and the specific contribution of *Ax* ($RE_{i,Ax}$), *OPBR* ($RE_{i,OPBR}$) and secondary settler ($RE_{i,SS}$) to wastewater treatment, were calculated according to equations 4-7 (Dhaouefi et al., 2018):

$$RE_{i,Ax}(\%) = \frac{(C_{i,SFWD} \cdot Q_{SFWD}) + (C_{i,OPBR} \cdot Q_{IR}) + (C_{i,E} \cdot Q_{ER}) - (C_{i,Ax} \cdot Q_{Ax})}{C_{i,SFWD} \cdot Q_{SFWD}} \cdot 100 \quad (4)$$

$$RE_{i,OPBR}(\%) = \frac{(C_{i,Ax} \cdot Q_{Ax}) - (C_{i,OPBR} \cdot Q_{OPBR}) - (C_{i,OPBR} \cdot Q_{IR})}{C_{i,SFWD} \cdot Q_{SFWD}} \cdot 100 \quad (5)$$

$$RE_{i,SS}(\%) = \frac{(C_{i,OPBR} \cdot Q_{OPBR}) - (C_{i,E} \cdot Q_{ER}) - (C_{i,E} \cdot Q_E) - (C_{i,E} \cdot Q_{WB})}{C_{i,SFWD} \cdot Q_{SFWD}} \cdot 100 \quad (6)$$

$$RE_{i,Ax-PBR}(\%) = \frac{(C_{i,SFWD} \cdot Q_{SFWD}) - (C_{i,E} \cdot Q_E)}{C_{i,SFWD} \cdot Q_{SFWD}} \cdot 100 \quad (7)$$

Where C_i accounts for TOC, IC, TN, NH_4^+-N and PO_4^{3-}-P concentrations in the SFWD, *Ax*, and *OPBR* . Q_{SFWD} represents the inlet flowrate, Q_{IR} represents the internal recirculation flowrate from *OPBR* to *Ax*, Q_{ER} stands for the external recirculation flowrate from the settler to *Ax* and Q_E represents the treated water flowrate. The water flow balances for the effluent (Q_E), the *Ax* (Q_{Ax})

and *OPBR* (Q_{OPBR}) are defined as $Q_E = Q_{SFWD} - Q_{Ev} - Q_{WB}$; $Q_{Ax} = Q_{SFWD} + Q_{RI} + Q_{RE}$ and $Q_{OPBR} = Q_{SFWD} + Q_{ER} - Q_{Ev} - Q_{IR}$. Q_{Ev} represents the evaporation flow rate, estimated as the difference between the daily flowrates of the feeding and effluent + wastage rate (Q_{WB}). Furthermore, carbon and nitrogen losses were quantified by means of the mass recovery factors for the parameter "i" according to equations 8, 9 and 10 (García et al., 2017a):

$$TC(\text{Recovery }\%) = \frac{M_{i,E}+M_{i,WB}}{M_{i,SFWD}} \cdot 100 = \frac{Q_E(TOC_E + IC_E + \%C \cdot TSS_E) + Q_{WB}(TOC_E + IC_E + \%C \cdot TSS_{WB})}{Q_{SWFD} \cdot (TOC_{SFWD} + IC_{SFWD})} \cdot 100 \quad (8)$$

$$TN(\text{Recovery }\%) = \frac{M_{i,E}+M_{i,WB}}{M_{i,SFWD}} \cdot 100 = \frac{Q_E(TN_E + \%N \cdot TSS_E) + Q_{WB}(TN_E + \%N \cdot TSS_{WB})}{Q_{SWFD} \cdot TN_{SFWD}} \cdot 100 \quad (9)$$

$$P(\text{Recovery }\%) = \frac{M_{i,E}+M_{i,WB}}{M_{i,SFWD}} \cdot 100 = \frac{Q_E(PO_4^{-3} - P_E + \%P \cdot TSS_E) + Q_{WB}(PO_4^{3-} - P + \%P \cdot TSS_{WB})}{Q_{SWFD} \cdot PO_4^{3-} - P_{SFWD}} \cdot 100 \quad (10)$$

where $M_{i,E,}$ and $M_{i,WB}$ represent the mass flow rate ($g \cdot d^{-1}$) of the parameter "i" (TC, TN and PO_4^{3-}-P) in the liquid effluent and waste biomass, respectively, and were defined as the mass flow rate of dissolved compounds (TOC + IC, TN or PO_4^{3-}-P) and mass flow rate of C, N, and P (determined by elemental composition) in the TSS of both the effluent and waste biomass. On the other hand, $M_{i,\,SFWD}$ stands for the mass flow rate of the parameter "i" in the influent SFWD. It was assumed that TC losses were associated to CO_2 volatilization, whereas TN losses corresponded to N_2 or NH_3 volatilization by denitrification or stripping, respectively. The TN lost as N_2 was estimated as the fraction of mass of NO_2^--N + NO_3^--N removed in *Ax*, whereas NH_3 was quantified as the remaining fraction of TN losses (not volatilized as N_2). Finally, the P recovery factor was used for validating the analytical and instrumental methodologies used in this study.

205 **2.6 DNA extraction, Illumina library preparation, pyrosequencing, and 16S rDNA-based**
206 **taxonomic analysis**

207 A sample was drawn for the analysis of the bacterial community structure from the cultivation
208 broth of *OPBR* during each steady-state. Total genomic DNA was extracted using the Fast DNA
209 Spin kit for soil (Biomedical, USA) according to the manufacturer's instructions. The extracted
210 DNA was stored at −20 °C prior to pyrosequencing. 5 $ng \cdot \mu L^{-1}$ in of genomic DNA in 10 mM Tris
211 pH 8.5 were used to start the Illumina protocol (Cod. 15044223 Rev. A), targeting the 16S rDNA
212 gene V3 and V4 region. The bacterial primers used were -D-Bact-0341-b-S-17 and S-DBact-0785-
213 a- A-21, forward and reverse, respectively, (Klindworth et al., 2012). Overhang adapter sequences
214 were added to the gene-specific sequences, thus resulting in the following full length 16S amplicon
215 PCR primers sequences: 5'TCGTCGGCAGCGTC
216 AGATGTGTATAAGAGACAGCCTACGGGNGGCWGCAG (forward) and 5′
217 GTCTCGTGGGCTCGGAGATGTGTATAAGAGAC-AGGACTACHVGGGTATCTAATCC
218 (reverse).

219 After 16S rDNA gene amplification, the mutiplexing step was performed using Nextera XT Index
220 Kit (FC-131-1096). 1 µl of the PCR product was run on a Bioanalyzer DNA 1000 (Agilent, USA)
221 chip to verify the size (~550 bp on a Bioanalyzer trace). After size verification, the libraries were
222 sequenced using a 2×300pb paired-end run (MiSeq Reagent kit v3 (MS-102-3001)) on a MiSeq
223 Sequencer according to instructions from the manufacturer (Illumina, San Diego, CA). The
224 pyrosequencing analysis was carried by the Foundation for the Promotion of Health and
225 Biomedical Research of Valencia Region (FISABIO, Spain). Quality assessment was performed
226 using the PRINSEQ-LITE program (Schmieder and Edwards, 2011), applying the following

parameters: min_length, 50; trim_qual_right, 30; trim_qual_type, mean; and trim_qual_window, 20. The bioinformatics analyses were performed in RStatistics environment. Metataxonomy analysis was performed using some of qiime2 plugins. Denoising, paired-ends joining, and chimera depletion were performed starting from paired ends data using DADA2 pipeline. Taxonomic affiliations were assigned using the Naive Bayesian classifier integrated with quiime2 plugins. SILVA_release_132 was used for taxonomic assignations. Krona representation was generated using Krona hierarchical browser (Ondov et al., 2011).

2.7 Statistical treatment

The results were provided as the mean and standard deviation of each parameter during steady-state periods. The differences in the means were statistically analyzed by t-test, One-Way ANOVA, and Tukey's post-hoc test using the software SPSS v.22.

3 Results and Discussion

3.1 Global performance

The anoxic-aerobic system supported a high removal of organic carbon with steady-state efficiencies of 92±2%, 96±1%, and 85%±3% during S-I, S-II, and S-III, respectively (F= 42.99, p= 0.000). Moreover, TN removal was also high and experienced no significant differences during S-I and S-II, achieving steady-state efficiencies of 84±3% and 79±6%, respectively, but decreased to 73±3% during S-III (F= 21.56, p=0.000). Similarly, the anoxic-aerobic system supported high removal efficiencies of PO_4^{3-}-P of 71±15% and 58±4% during S-I and S-II, respectively, but a significantly lower removal of 28±16 % was observed in S-III (F= 12.93, p= 0.001). Overall, the system provided consistent removal efficiencies when compared to previous works using anoxic-

aerobic systems for the treatment of municipal wastewater (TOC, TN and PO_4^{3-}-P removal efficiencies of 86-95%, 18-87%, and 22-67%, respectively)(de Godos et al., 2014; Alcántara et al., 2015a; García et al., 2017a; Toledo-Cervantes et al., 2019), or during the treatment of textile wastewater (TOC: 45-52%, TN:10-87%)(Dhaouefi et al., 2018). High removal efficiencies were fostered by a high photosynthetic activity, promoted by the high HRT and SRT of operation and the high nutrients availability from the SFWD. These results confirmed the potential of this technology for the treatment of high-strength wastewaters with the concomitant production of valuable microalgal-bacterial biomass.

Microalgae and bacteria in *Ax* and in *OPBR* contributed to the transformation and removal of carbon, nitrogen, and phosphorus using multiple mechanisms. The symbiosis between microalgae and bacteria resulted in the biological oxidation of TOC in both *Ax* and *OPBR*, whereas assimilation/nitrification and denitrification in the *OPBR* and *Ax*, respectively, supported the high TN removals observed. The denitrification-nitrification configuration operated under high HRT and SRT (Table 1) likely attenuated the inhibitory effect on the microbial communities mediated by the high ammonia concentrations and pH of the SFWD, which is one of the main constrains reported for microalgae-based treatment of high-strength wastewaters (Stiles et al., 2018). In addition, the autotrophic activity of microalgae and nitrifying bacteria was enhanced by the high influent IC concentrations. In this context, global steady-state IC removal efficiencies of 52±5%, 65±11%, and 37±14% were recorded in S-I, S-II, and S-III, respectively. At the pH prevailing in *Ax* and *OPBR*, IC was available for autotrophic activity mainly in the form of HCO_3^-, which is an assimilable form for both microalgae (White et al., 2013) and nitrifiers (Wett et al., 2003), as described for food waste digestate for microalgae cultivation (Chuka-Ogwude et al., 2020) and confirmed in this study. The availability of inorganic carbon was herein influenced by the changes

in pH in *OPBR* along the different operational stages. For instance, the high pH values in this unit during S-I likely resulted in a displacement of the CO_2 equilibrium to carbonate, which reduced the availability of the influent IC. The decrease in pH during S-II and S-III induced by the increase in SFWD load enhanced the availably of inorganic carbon and likely intensified the stripping of CO_2 (Table 1) in *OPBR*, which ultimately resulted in lower TC recoveries during these stages (53±11% and 45±9% during S-II and S-III, respectively, compared to 88±13% during S-I). Additionally, the availability of IC from the influent SFWD and the biodegradation of TOC in *Ax* favored the removal of nitrogen.

The global TN removal was directly linked to the removal of NH_4^+-N, which presented average steady-state values higher than 99% due to the occurrence of intensive nitrification during S-I and S-II. Simultaneous organic carbon removal and nitrification were supported by the active photo-oxygenation in *OPBR*, as suggested by the pH and DO of 9.7±0.1 and 14±5 $mg \cdot L^{-1}$ during S- I and 8.9±0.2 and 2.8±2.7 $mg \cdot L^{-1}$ during S-II, respectively (Table 1, Figure 2a and 2b). The increase in SFWD pollutant concentrations during S-III caused a lower NH_4^+-N removal of 73±10% as a result of the depletion of DO in *OPBR* during this stage, which showed average concentrations of 0.01±0.00 $mg \cdot L^{-1}$. Intensive denitrification occurred during S-I and S-II in *Ax* since DO concentrations remained low (<0.04 $mg \cdot L^{-1}$) throughout the experiment. Nitrification and denitrification were also favored by the long operational HRT and SRT, which prevented the wash-out of nitrifiers as reported elsewhere (Rada-Ariza et al., 2017).

Table 1. Operational conditions and steady-state process parameters (average values ± standard deviations) of the anoxic–aerobic system during the treatment of SFWD.

Parameter	Sample	Stage		
		S-I (N=8)	S-II (N=8)	S-III (N=8)
TOC ($mg \cdot L^{-1}$)	SFWD	218 ± 14	433 ± 23	815 ± 35
	Ax	33 ± 5	42 ± 15	291 ± 37
	OPBR	25 ± 8	34 ± 10	229 ± 48
	E	27 ± 7	36 ± 9	189 ± 40
IC ($mg \cdot L^{-1}$)	SFWD	168 ± 10	318 ± 13	599 ± 23
	Ax	158 ± 13	268 ±14	652 ± 44
	OPBR	114 ±11	197± 16	628 ± 49
	E	123 ± 9	199 ± 12	613 ± 49
TN ($mg \cdot L^{-1}$)	SFWD	143 ± 10	306± 10	610 ± 23
	Ax	47 ± 5	126 ± 22	333 ± 26
	OPBR	34 ± 5	87 ± 31	247 ± 35
	E	32 ± 4	81 ± 30	232 ± 32
NH_4^+-N ($mg \cdot L^{-1}$)	SFWD	74 ± 15	177 ± 14	385 ± 34
	Ax	24 ± 5	50 ± 5	236 ± 77
	OPBR	1 ± 0	1 ± 0	169 ± 55
	E	1 ± 0	2 ± 2	139 ± 46
NO_2^--N ($mg \cdot L^{-1}$)	SFWD	0	0	0
	Ax	10 ± 4	22 ± 14	0 ± 0
	OPBR	4 ± 3	24 ± 8	0 ± 1
	E	5 ± 4	23 ± 8	0 ± 1
NO_3^--N ($mg \cdot L^{-1}$)	SFWD	0	0	0
	Ax	7 ± 6	21 ± 9	0 ± 0
	OPBR	28 ± 7	68 ± 23	0 ± 1
	E	26 ± 7	62 ± 18	0 ± 0
PO_4^{3-}-P ($mg \cdot L^{-1}$)	SFWD	10 ± 1	22 ± 1	46 ± 11
	Ax	7 ± 4	13 ± 2	41 ± 4
	OPBR	3 ± 3	12 ± 1	42 ± 4
	E	4 ± 2	13 ± 2	48 ± 52
pH	SFWD	8.4 ± 0.2	8.5 ± 0.1	8.5 ± 0.2
	Ax	8.6 ± 0.2	8.3 ± 0.2	8.5 ± 0.1
	OPBR	9.7 ± 0.1	8.9 ± 0.2	8.7 ± 0.1
	E	9.4 ± 0.1	9.0 ± 0.1	8.9 ± 0.1
DO	*Ax*	0.02 ± 0.03	0.03 ± 0.02	0.01 ± 0.00
	OPBR	14 ± 5	2.8 ± 2.7	0.01 ± 0.00
HRT (d)	*Ax*	2.4	2.4	2.4
	OPBR	7.6	7.6	7.6
SRT (d)		19 ± 4	19 ± 6	26 ± 5
TC (Recovery %)		88 ± 13	53 ± 11	45 ± 9
TN (Recovery %)		44 ± 8	36 ± 8	32 ± 5
P (Recovery %)		111 ± 15	109 ± 4	107 ± 8
Exp. Period		40	47	54

The extent of nitrogen losses via denitrification or NH_3 volatilization was estimated by means of the TN recovery factors, which averaged 44±8%, 36±8%, and 32±5% during S-I, S-II, and S-III, respectively (Table 1). In this context, the mass flowrate of NO_3^--N removed in *Ax* amounted 0.05±0.02 and 0.11±0.06 $g \cdot d^{-1}$ during S-I and S-II, respectively, corresponding to 32±13% and

296 31±15% of the influent TN, which were ultimately denitrified during these stages. Hence, the
297 shares of volatilized NH_3 were 23±15% and 33±20% during S-I and S-II, respectively. Since no
298 NO_3^--N was produced during S-III in *OPBR*, denitrification was negligible during this stage, and
299 68±4% of the influent TN was likely volatilized from the system in the form of NH_3.

300 The high PO_4^{3-}-P removal efficiencies recorded during SI and SII were mediated by P assimilation
301 into microalgal-bacterial biomass since the pH values recorded in *OPBR* remained below 10,
302 which is typically required to support active phosphate precipitation (Alcántara et al., 2015a;
303 García et al., 2017a). The P mass balance showed average recovery factors during the experimental
304 period of 109±12%, which validated the analytical and instrumental methodologies used in this
305 study (Table 1). Finally, steady-state biomass concentrations (Figure 2c) averaged 1.0±0.1,
306 1.0±0.2 and 0.5±0.1 g VSS·L^{-1} in *Ax*, and 0.9±0.1, 1.1±0.1 and 1.0±0.1 g VSS·L^{-1} in *OPBR* during
307 S-I, S-II, and S-III, respectively. The decrease in VSS concentrations in *Ax* during S-III ($F=31.10$,
308 $p=0.000$, S-III<S-II, Tukey's comparison) was correlated with the decrease in TOC, NH_4^+-N and
309 PO_4^{3-}-P removal efficiencies mediated by the use of undiluted SFWD, which entailed a DO
310 depletion in the *OPBR* (limiting organic matter oxidation) and a poor settling of the microalgal-
311 bacterial biomass (as shown by the increase in VSS concentration in the effluent) (Figure 2c).

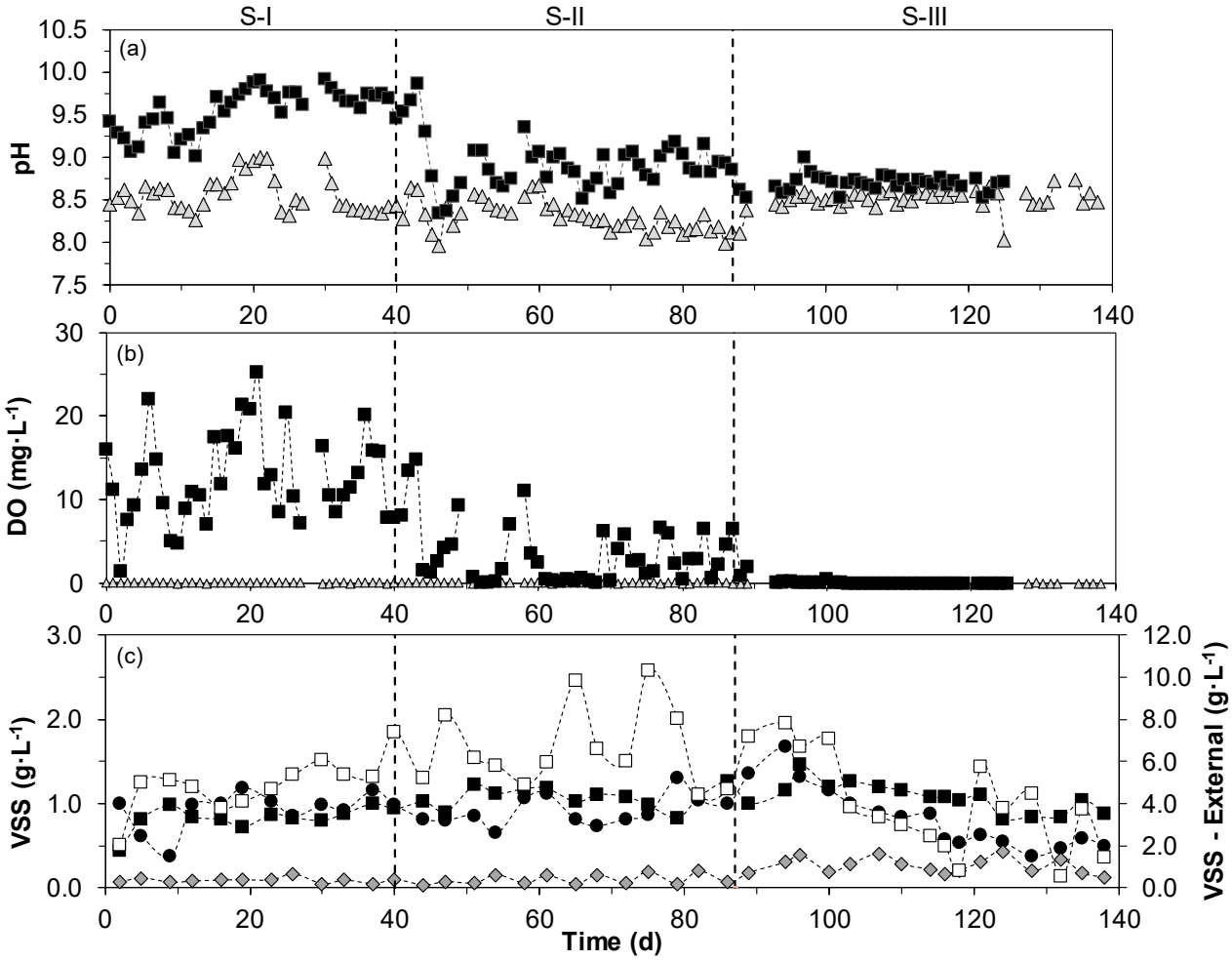

Figure 2. Time course of (a) pH and (b) dissolved oxygen concentration (DO) in the (▲) anoxic reactor (*Ax*) and (■) open photobioreactor (*OPBR*); and (c) VSS concentrations in (▲) *Ax*, (■) *OPBR*, (□) external recirculation and (◆) final effluent (*E*).

3.2 Carbon and nutrient removal in the anoxic reactor

Ax contributed with steady-state TOC removal efficiencies of 76±8%, 87±6%, and 44±5% during S-I, S-II, and S-III, respectively (Figure 3a and 3b), coinciding with the range of 65 –77% reported in previous works (Alcántara et al., 2015, Garcia et al., 2017). TOC removal in *Ax* was mediated by organic carbon uptake by facultative bacteria and heterotrophic denitrification using the NO_2^--N/NO_3^--N recirculated from *OPBR*, mainly in S-I and S-II. In fact, the deterioration in TOC removal during S-III coincided with the loss of nitrification in *OPBR*, which stopped the NO_2^--N and NO_3^--

N supply to *Ax* (Figure 4). The TOC removal efficiency of 44±5% observed during S-III in *Ax* was attributed mainly to carbon uptake by facultative bacteria. Overall, TOC absorption in this unit may have been favored by the starvation of the microalgal-bacterial biomass in the settler. On the other hand, negative steady-state IC removal efficiencies of -57±37%, -38±8%, and -21±7% (Figure 3c and 3d) were measured in *Ax* due to the release of CO_2 from TOC oxidation in this unit, which also contributed to the recovery of IC in the cultivation broth typically attributed to denitrification (Elefisionitis et al., 2004).

Denitrification in *Ax* was the main mechanism of nitrogen removal during S-I and S-II and was supported by the influent TOC available for heterotrophic consumption during denitrification, as suggested by the TOC/NO_3^--N ratios of 3-8 and 2-6 observed during S-I and S-II (Bernet et al., 1996). Figure 4 shows the concentrations of NO_2^--N and NO_3^--N in *Ax*, which presented steady-state values of 10±4, 22±14 and 0±0 mg·L^{-1}, and 7±6, 21±9 and 0±0 mg·L^{-1} during S-I, S-II, and S-III, respectively. The internal and external recirculation represented the main inputs of NO_2^--N and NO_3^--N to *Ax*, which were supported by the active nitrification in *OPBR*. Furthermore, a partial reduction of NO_3^--N to NO_2^--N likely mediated by the slightly alkaline conditions in *Ax* (Si et al., 2018) might explain the remaining NO_2^--N concentrations in this unit. During S-III, the DO depletion in *OPBR* resulted in negligible NO_2^--N and NO_3^--N concentrations under steady-state, which prevented the occurrence of denitrification in *Ax*. Overall, *Ax* provided TN removal efficiencies of 43±9% (S-I), 35±10% (S-II), and 10±4% (S-III). Similar efficiencies (11-63%) were reported by Alcántara et al. (2015) and García et al. (2017), also mediated by NO_2^--N and NO_3^--N reduction. In addition, NH_4^+-N removal efficiencies of -9±19%, 4±10%, -10±43% were measured under steady-states during S-I, S-II, and S-III, respectively (Figure 5a, 5b). These removals of TN and NH_4^+-N suggest that besides denitrification, other nitrogen transformation

processes also took place in the *Ax*. Thus, a preferential assimilation of the organic nitrogen present in the SFWD, certain ammonification, or even NO_2^--N/NO_3^--N dissimilation to NH_4^+-N induced by the low DO concentrations likely occurred during S-I and S-II in *Ax* (Figure 5c, 5d).

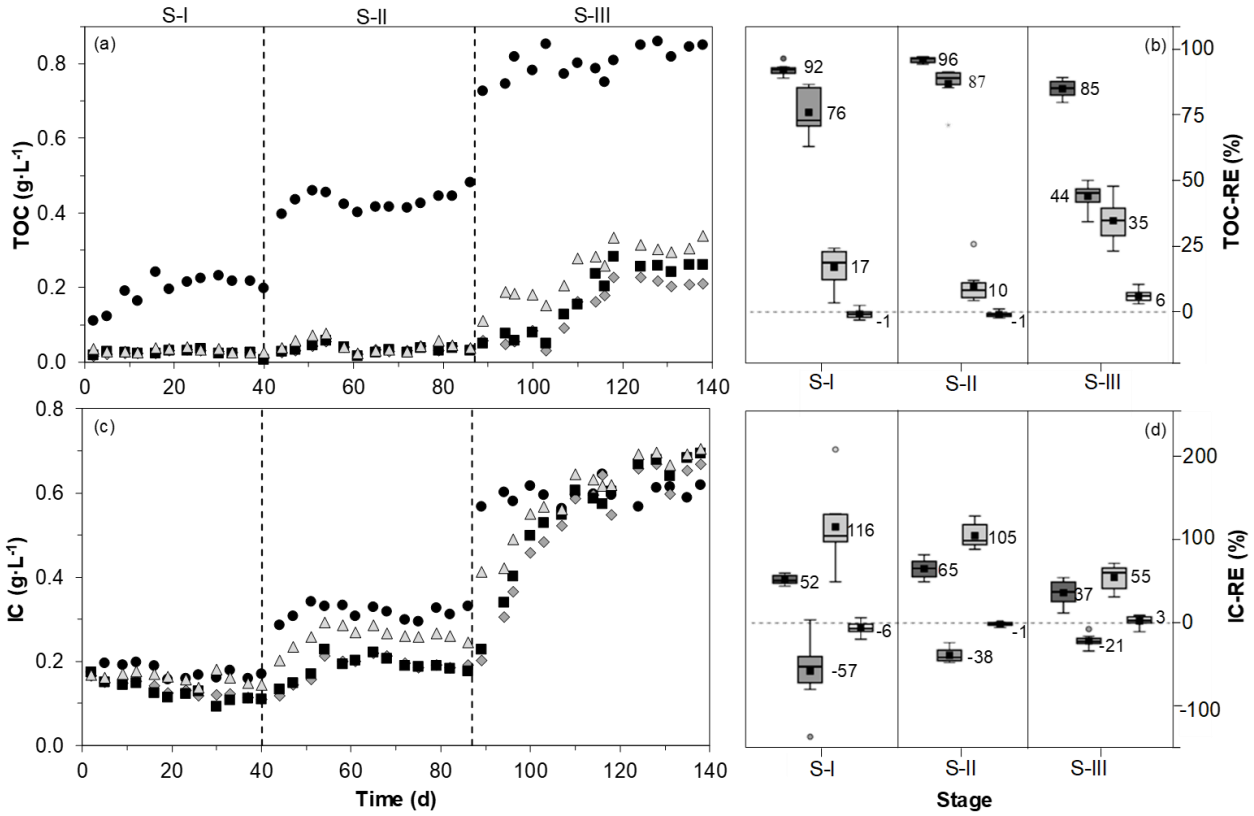

Figure 3. Time course of (a) TOC concentration and (b) boxplot for the TOC removal efficiency in the overall system (■), anoxic reactor (*Ax*), (▭) open photobioreactor (*OPBR*), (▭) and secondary settler (▭); (c) IC concentrations; d) boxplot for the IC removal efficiency in the overall system (■), *Ax* (▭) and *OPBR* (▭) and secondary settler (▭). (●) influent SFWD, (▲) *Ax*, (■) *OPBR* and (◆) final effluent (*E*).

Finally, *Ax* provided steady-state phosphate removal efficiencies of -70±96%, 19±40%, and 22±14% during S-I, S-II, and S-III, respectively (Figure 5e, 5f). Similarly to the observations of García et al. (2017a), the negative PO_4^{3-}-P removals recorded during S-I suggested that P was released by the recycled microalgal-bacterial consortium in the absence of DO. In this context, recent studies have reported the ability of microalgae to accumulate non-structural PO_4^{3-}-P under aerobic conditions, which is then released in the absence of oxygen (Solovchenko et al., 2016).

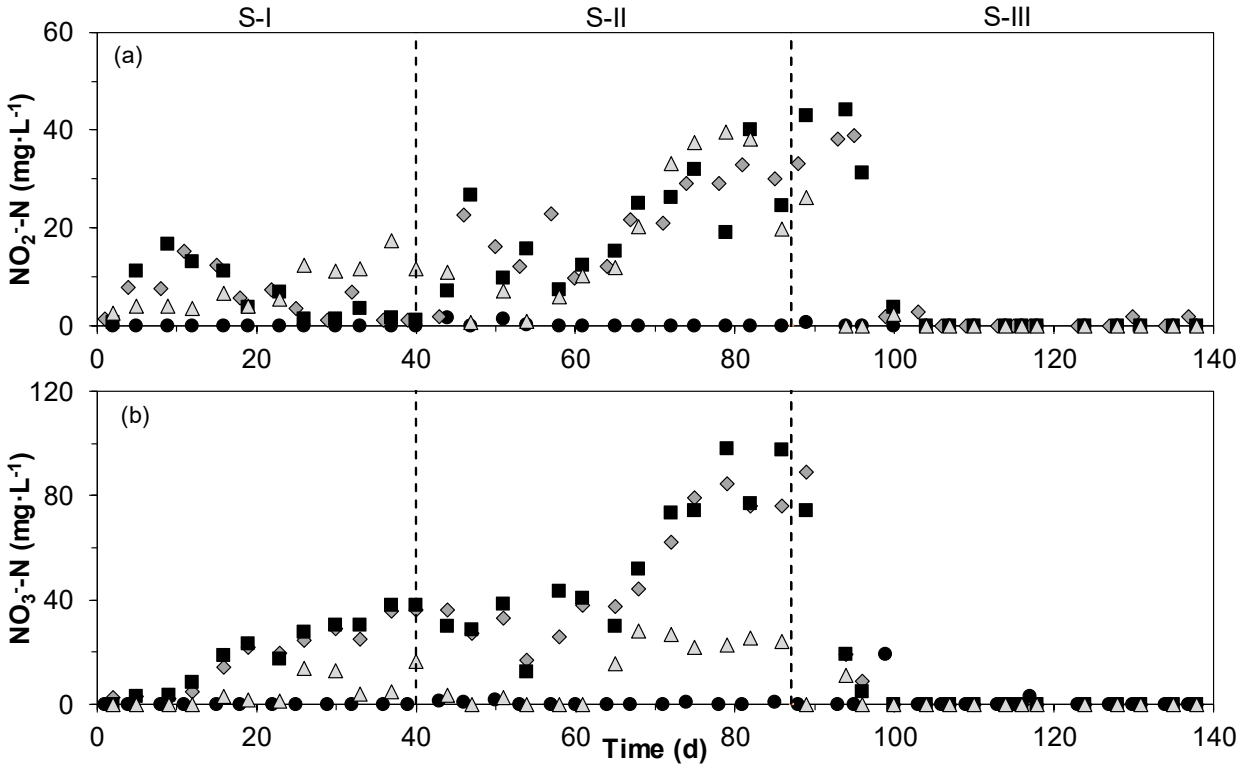

360

361 **Figure 4.** Time course of the concentration of (a) NO_2^--N and (b) NO_3^--N in the (●) influent SFWD, (▲)
362 anoxic reactor (*Ax*), (■) open photobioreactor (*OPBR*), and (◆) final effluent (*E*).

363 **3.3 Carbon and nutrient removal in the open photobioreactor**

364 *OPBR* contributed with steady-state TOC removal efficiencies of 17±10%, 10±6%, and 35±8%
365 during S-I, S-II S-III, respectively, in agreement with previously reported efficiencies (24– 32%,
366 Alcántara et al., 2015; García et al., 2017). The efficient TOC removal in *Ax* resulted in the most
367 recalcitrant soluble TOC entering *OPBR*, which efficiently removed this residual organic matter.
368 The TOC in the final effluent corresponded to 8%, 4%, and 13% of the influent TOC and to
369 concentrations in the final effluent of 27±7, 36±9, and 189±40 mg TOC·L^{-1} during S-I, S-II, and
370 S-III, respectively. These concentrations were attributed to the incomplete degradation of the
371 potassium hydrogen phthalate (KHP) present in the SFWD. Overall, the low biodegradability of
372 the SFWD, evidenced by a TOC:COD ratio of 0.33 and a C:N ratio of 1.2, did not limit the activity
373 of the microalgal-bacterial consortium, which consumed most of the influent organic carbon.

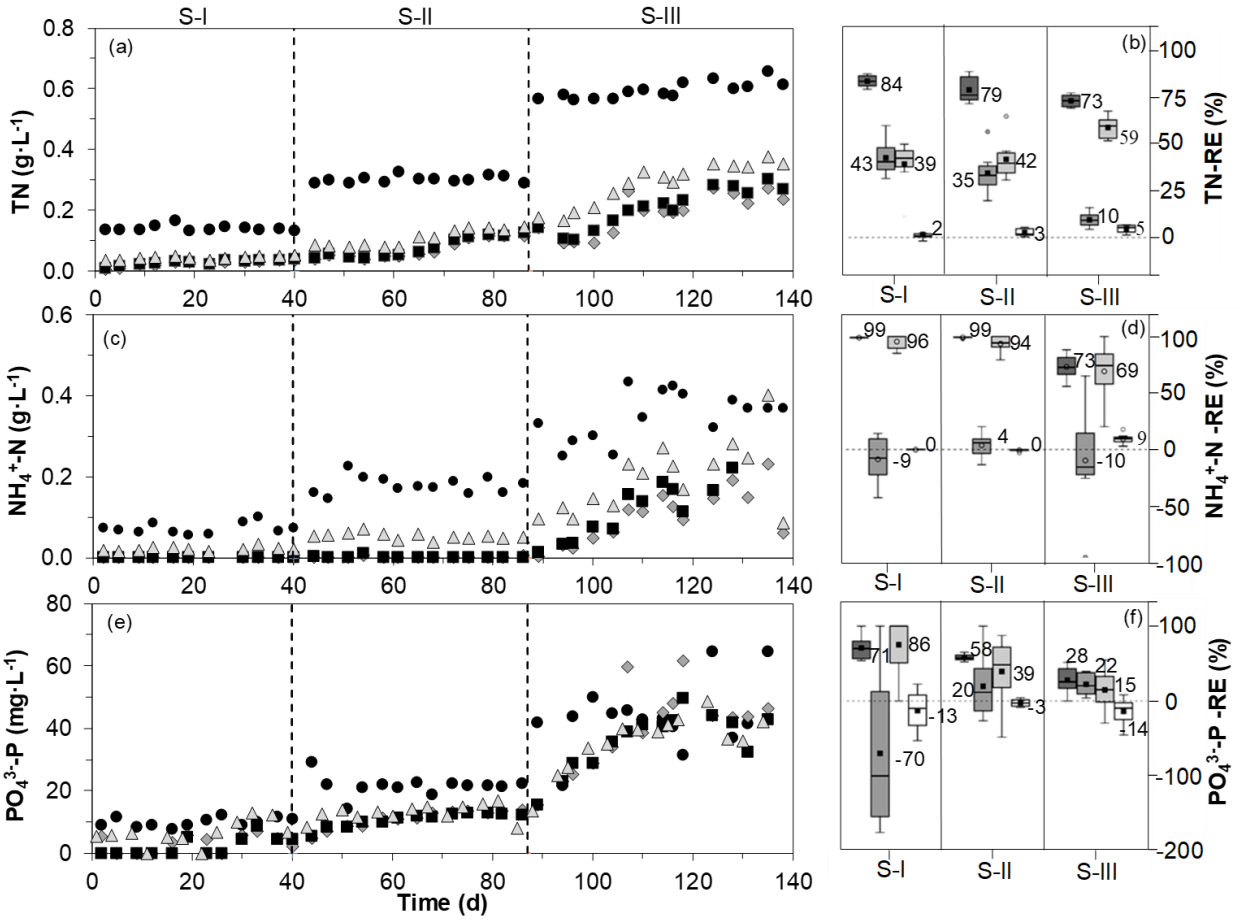

Figure 5. Time course of (a) TN concentrations and (b) boxplot for the TN removal efficiencies of the overall system (■), anoxic reactor (*Ax*), (▤), open photobioreactor (*OPBR*), (▭) and secondary settler (▭); (c) NH_4^+-N concentrations, (d) boxplot for NH_4^+-N removal efficiencies of the overall system (■), *Ax* (▤), *OPBR* (▭) and secondary settler (▭); (e) PO_4^{3-}-P concentrations (f) boxplot for PO_4^{3-}-P removal efficiencies of the overall system (■), *Ax* (▤), *OPBR* (▭), and secondary settler (▭). (●) influent SFWD, (▲) *Ax*, (■) *OPBR,* and (◆) final effluent (*E*).

The high IC removal efficiencies in *OPBR* accounted respectively for 116±42%, 105±14%, and 55±14% in S-I, S-II, and S-III, which revealed the intensive autotrophic activity (active consumption of CO_2) of microalgae and nitrifiers in the photobioreactor during the illuminated period along the three operational stages. The removal efficiencies higher than 100% in *OPBR* can be explained by the IC released during denitrification in *Ax* and the fact that they were estimated based on the influent IC mass flow rate. Hence, the inorganic carbon present in SFWB or generated from TOC oxidation was assimilated during photosynthetic growth of microalgae and also

consumed during nitrification in order to support NH_4^+-N removal efficiencies of 96±6%, 94±7%, and 69±23% (corresponding to 8.8, 22.9, and 36.1 g NH_4^+-N $m^{-3}d^{-1}$ removed in S-I, S-II, and S-III, respectively). The oxidation of NH_4^+-N resulted in the production of NO_2^--N (under partial nitrification) and NO_3^--N (full nitrification). Steady-state effluent NO_2^--N concentrations averaged 5±4, 23±8, and 0±1 mg·L^{-1} in Stages I, II, and III, whereas effluent NO_3^--N concentrations reached 26±7, 62±18, 0±0 mg·L^{-1}, respectively. In this context, the remaining concentrations of IC and NH_4^+-N in the mixed liquor of *OPBR* suggested that enough inorganic carbon and nitrogen were available for both nitrification and microalgae growth in S-I and S-II, even under conditions of active competition between microalgae and nitrifiers. Additionally, as previously observed by Gonzales-Camejo et al. (2018), the temperature in the *OPBR* and the high SRT (>2.5 d) supported microalgae and nitrifiers activity without severe restrictions during S-I and S-II.

Oxygen limitation was the main reason for the interruption of nitrification during S-III since the increase in influent TOC to 815±35 mg·L^{-1} and NH_4^+-N to 385±34 mg·L^{-1} mediated a very high demand of oxygen, exceeding the photo-oxygenation capacity of microalgae. Negative Spearman correlations were observed between DO and the concentrations of TN (r_s= -0.83, p=0.00) and NH_4^+-N (r_s=-0.84, p=0.00) in *OPBR*, thus supporting the hypothesis of oxygen-limited nitrification. TN removal efficiencies in *OPBR* averaged 39±11%, 42±10%, and 59±5% in stages I, II, and III, respectively. Additionally, NH_4^+-N in the final effluent remained below 1% of the influent NH_4^+-N during S-I and S-II, but increased up to 23% during S-III. The adjustment of influent loading rates is a feasible strategy for maintaining photo-oxygenation and high removal efficiencies during the treatment of high influent TOC and TN concentrations, such as those prevailing during S-III. These high concentrations could be treated under lower loading rates (*i.e.*, 43.3 g TOC·m^{-3}·d^{-1} and 30.6 g TN·m^{-3}·d^{-1}, S-II, for which a higher HRT of 18 d would be required).

411 Volatilization of NH_3-N accounted for 23±15% and 33±20% of the nitrogen removed during S-I
412 and S-II but increased up to 68±4% during S-III, fostered by DO depletion in *OPBR* and the
413 subsequent inhibition of the nitrification-denitrification process in this stage. As reported by
414 González-Fernández et al. (2011), the increase in influent loading rates of NH_3-N under
415 unfavorable conditions for nitrification-denitrification resulted in higher losses by stripping.
416 Assimilation into microalgal-bacterial biomass was also responsible for nitrogen transformation
417 and removal. The shares of the influent TN assimilated in the form of biomass accounted for
418 30±7%, 15±4%, and 5±2% during S-I, S-II, and S-III, respectively. Both NH_4^+-N and NO_3^--N are
419 nitrogen forms that can be assimilated by microalgae, although ammonium is preferred since its
420 assimilation is thermodynamically more favorable (Cai et al., 2013). In this context, the
421 assimilation of NH_4^+-N by microalgae and bacteria limited nitrification during S-I and S-II, and
422 together with volatilization, sustained nitrogen removal during S-III, where nitrification was
423 seriously hampered. Microalgae are efficient competitors for ammonium for nitrifiers since these
424 photosynthetic microorganisms have higher N uptake and growth rates (Risgaard-Petersen et al.,
425 2004). Moreover, NH_3-mediated inhibition of microalgae and nitrifiers represents a challenge
426 during the treatment of high-strength wastewaters, including food waste digestate. In our particular
427 study, the concentrations of NH_4^+-N measured in *OPBR* amounted 1±0, 2±3, and 169±55 $mg \cdot L^{-1}$,
428 during S-I, S-II, and S-III, respectively. The average pH in the same stages in *OPBR* was 9.7±0.1,
429 8.9±0.2, and 8.7±0.1, resulting in estimated fractions of free ammonia of 81.2%, 31.6%, and 7.7%
430 and NH_3-N concentrations of 0.6±0.3, 0.4±0.1, and 46±14 $mg \cdot L^{-1}$ (Figure S1). These
431 concentrations were not inhibitory of microalgae growth in *OPBR* during the initial stages but
432 likely contributed to the overall decrease in VSS concentration observed during S-III. Table S1
433 presents an overview of the different mechanisms involved in nitrogen transformation in the
434 anoxic-aerobic system.

435 Finally, the removal of orthophosphates accounted for 86±31%, 39±41%, and 15±26% of the
436 influent load under steady-state in S-I, S-II, and S-III, respectively (Figure 5e, 5f). Phosphorus
437 assimilation by the microalgal-bacterial biomass was the main removal mechanism in *OPBR* based
438 on the range of pH values recorded throughout the experimental period. In this sense, phosphorus
439 uptake rates in *OPBR* accounted for 0.4±0.3, 0.4±0.2, and 0.4±0.3 g PO_4^{3-}-P·m^{-2}·d^{-1} during S-I, S-
440 II, and S-III, respectively. These rates were higher than those reported in microalgal biofilms
441 treating municipal wastewater (Boelee et al., 2011).

442 **3.4 Contribution of the secondary settler**

443 The main contribution of the settler was the separation of the biomass from the OPBR, which
444 resulted in TSS concentrations in the final effluent of 95±31, 113±67, and 347±135 mgL^{-1},
445 corresponding to removal efficiencies of 98±1% (S-I), 99±1% (S-II) and 96±2% (S-II),
446 respectively. These results showed the high settleability of the biomass, as previously reported by
447 Toledo-Cervantes et al. (2019), even in S-III, when the loss of photo-aeration capacity resulted in
448 an increase in the solids in the effluent. Furthermore, the occurrence of carbon, nitrogen, and
449 phosphorus transformation processes in the secondary settler was also quantified. Interestingly,
450 this unit contributed with TOC and TN removal efficiencies below 2% during S-I and S-II, but with
451 6±2% and 5±2%, respectively, during S-III, enhancing the performance of the system (Figure 3b
452 and 5b). The removal of TOC was attributed to the activity of heterotrophic bacteria, even during
453 the biomass separation, with a concomitant release of CO_2 that explains the slight negative removal
454 of IC of -6±7% and -1±2% during S-I and S-II (Figure 3d). On the other hand, the removal of TN
455 was associated with NH_3 volatilization induced by the high pH of the effluent, mainly during S-III
456 (9.0±0.1), evidenced by the NH_4^+-N removal (Figure 5d), which was negligible during S-I and S-
457 II but presented values of 9±4% during S-III. Finally, the environmental conditions prevailing in

458 the settler also contributed to a certain P release since negative PO_4^{3-}-P removal efficiencies of -
459 18±26%, -3±4%, and -14±17% were measured during S-I, S-II, and S-III, respectively (Figure 5f).

460 **3.5 Microalgae and bacteria populations**

461 The species dominating the microalgae community of *OPBR* during the experimental period
462 belonged to three phyla: Chlorophyta (*Chlorella vulgaris*, *Chlorococcum* sp., *Tetracoccus* sp. and
463 *Tetradesmus obliquus*), Cyanobacteria (*Aphanothece* sp., *Pseudoanabaena* sp), and Cryptophyta
464 (*Cryptomonas* sp.). Microalgae were present at concentrations of 2.4×10^{10}, 1.8×10^{10}, and 6.5×10^{9}
465 cell·L^{-1} in *OPBR* during S-I, S-II, and S-III (Figure 6a). The treatment of 4-fold diluted digestate
466 (25%) during S-I resulted in the increase in microalgae densities with respect to the initial
467 inoculum (1.3×10^{10} cell·L^{-1}), showing a beneficial effect of the diluted digestate on microalgae
468 growth. Nevertheless, the further increase in digestate loads resulted in decreases of 27% and 63%
469 in the microalgae densities during S-II and S-III compared to Stages S-I and S-II, respectively. The
470 number of microalgae cells per gram of VSS and microalgae biovolume also decreased when
471 increasing the loading rate (Figure 6a). Thus, the treatment of undiluted digestate (which resulted
472 in concentrations of 46±14 mg NH_3-N·L^{-1} in the mixed liquor of *OPBR* during S-III) contributed
473 to the severe loss of microalgae, reducing photo-aeration and hampering nitrification capacity and
474 bacterial respiration. Thus, NH_3-N concentration in *OPBR* was a major driver of microalgae
475 densities (r_s=-0.88, p= 0.033) and likely fostered the dominance of *Chlorella vulgaris* and
476 *Pseudoanabaena* sp. during S-III compared to the dominance of *C. vulgaris*, *Tetradesmus*
477 *obliquus,* or *Cryptomonas* sp. in S-I and S-II (Figure 6b). The dominance of *C. vulgaris* and
478 *Pseudoanabaena* sp. has been reported in previous works in anoxic-aerobic systems during the
479 treatment of municipal and textile wastewaters (Alcántara et al., 2015b; Dhaouefi et al., 2018) and

attributed to their tolerance to high ammonia concentrations (Collos and Harrison, 2014; Gutiérrez et al., 2016).

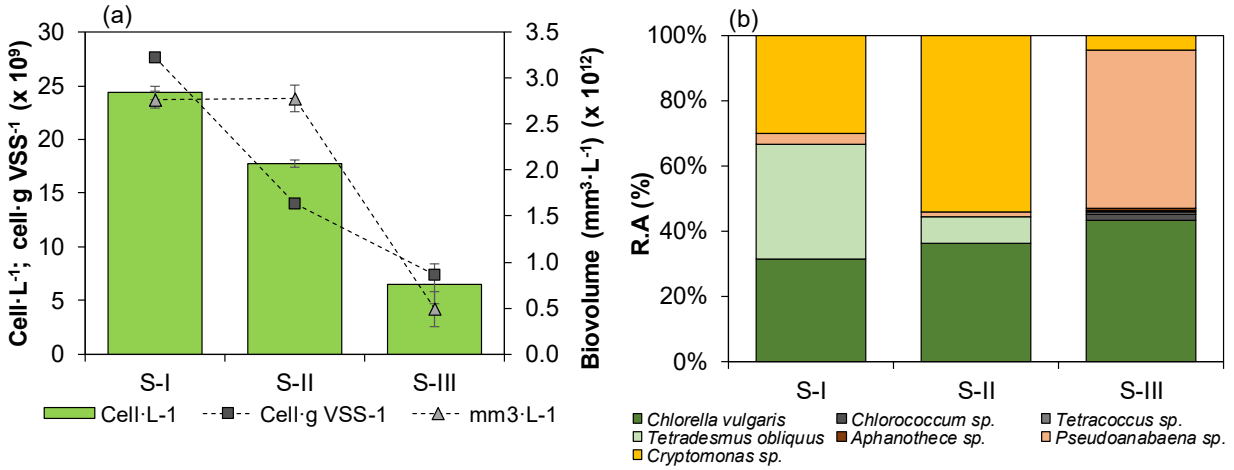

Figure 6. (a) Total microalgae densities per L and per gram of VSS, and total microalgae biovolume and (b) Relative abundances (R.A) per species of the main phyla of microalgae in the open photobioreactor during Stages I (S-I), II (S-II) and III (S-III).

On the other hand, a total of 105904, 77947, and 126926 16S rRNA sequence reads were retrieved and passed the quality and taxonomic cut-off for the samples from S-I, S-II, and S-III, respectively. The bacterial diversity was affiliated to 260 OTUs, distributed in 19 phyla during S-I and S-III, and 16 phyla during S-II. The main phyla dominating the bacterial community were Proteobacteria, Planctomycetes, Bacteroidetes, Firmicutes, and Verrucomicrobia, which accumulated 87%, 90%, and 95% of the relative abundances during S-I, S-II, and S-III. Among them, *Proteobacteria* was the most abundant phyla, representing 41% and 72% of the relative abundance in S-I and S-II, followed by *Planctomycetes*, with 43% and 9%, respectively. In the S-III, *Proteobacteria* (55%) and *Bacteroidetes* (27%) were the most dominant phyla. At the class level, the most representative groups were *Alpha- and Gammaproteobacteria*, with relative abundances of 25%, 68%, and 7%, and 16%, 4%, and 48%, during S-I, S-II, and S-III, respectively. Additionally, *Planctomycetacia* (*Planctomycetes)* exhibited shares of 43% and 9% during S-I and S-II but decayed to 0% in the S-III, when a high abundance of 27% for *Bacteroidia* (*Bacteroidetes)*

499 was detected. *Alpha*- and *Gammaproteobacteria, Planctomycetacia,* and *Bacteroidia* are included
500 among dominant classes in high rate algal ponds (Ibekwe et al., 2017). Additionally, Chao1
501 presented values of 185, 110, and 179, whereas the Shannon -Wiener indexes were 3.38, 1.87, and
502 3.01, during S-I, S-II, and S-III, respectively, in accordance with the typical values recorded
503 wastewater treatment systems (Chen et al., 2020). The lower diversity during S-II suggested that
504 a more specialized bacterial community (Pascual et al., 2020) dominated the system compared to
505 that of S-I, whilst the depletion of oxygen in *OPBR* during S-III supported the growth of facultative
506 organisms and the subsequent increase in bacterial diversity.

507 The dominant genera in each stage also contributed to elucidate the role of the bacterial
508 communities in the transformation of digestate pollutants. The sequencing showed a total of 153,
509 95, and 152 genera in S-I, S-II, and S-III, respectively (Figure 7c, 7d, 7e). Of them, 19, 10, and 14
510 genera presented relative abundances higher than 1%, accumulating 40%, 22%, and 40% of the
511 bacterial abundance of S-I, S-II, and S-III, respectively. The dominance of *Gemmata* (20%) and
512 the high presence of *Planctomicrobium* (16%) and *Legionella* (9%) (associated with organic
513 carbon transformation in aerobic environments, Chouari et al., 2003; Caicedo et al., 2020; Ali et
514 al., 2020), along with the presence of *Terrimicrobium* and members of *Caldilineaceae* (which
515 support carbon transformation under anoxic conditions, Liu and Li, 2019), suggest that these
516 bacteria were responsible for carbon removal in both *Ax* and *OPBR* in S-I. The high abundance of
517 *Azospirillum* (60%) during S-II, which can grow heterotrophically, symbiotically associated with
518 microalgae during the treatment of wastewater containing ammonium and phosphorus (de-Bashan
519 et al., 2002), suggested a high specialization of the microalgal-bacterial consortia induced by the
520 increase in digestate load, as also indicated by the lower value of the Shannon –Wiener index
521 compared to S-I. The treatment of undiluted digestate in S-III resulted in the dominance of

Psychrobacter, whose presence has been reported in microalgal-bacterial photobioreactors (García et al., 2017b). However, the increasing presence of organisms found under anoxic/anaerobic conditions, such as *Rikenellaceae* (13%) and *Firmicutes* (3%), was a result of the depletion of oxygen in *OPBR* during this stage (Lee et al., 2018; Yi et al., 2014) (Figure S2a – Supplementary material).

Finally, bacterial sequencing also allowed the detection of bacteria belonging to the nitrogen cycle (Figure S2b – Supplementary material). At least 28 genera were related to nitrogen transformation, which accumulated low abundances of 7%, 7%, and 6% during S-I, S-II, and S-III. Similar relative abundances of these organisms have been previously reported in anoxic-aerobic systems (How et al., 2019), as a result of the dominance of carbon removal bacteria. In this study, most bacteria responsible for nitrogen transformations were organisms previously reported as denitrifiers in systems with simultaneous nitrification and denitrification or denitrification in bioreactors inoculated with activated sludge or sediments, such as *Pirellula*, *Paracoccus*, *Bosea,* and *Devosia* (Feng et al., 2017; Xia et al., 2019; Feng et al., 2020), which were present during all stages. In the S-I, nitrifying organisms such as *Pirellulaceae* (Kellogg et al., 2016) and *Aeromonas* (García et al., 2017b) were identified, whereas *Nitrosomonas* was more abundant in S-II and S-III. *Alcaligenes* and *Chryseobacterium,* organisms capable of conducting a simultaneous nitrification-denitrification, were also present in S-II and S-III (Kundu et al., 2014; Shoda and Ishikawa, 2014). The role of heterotrophic denitrifiers was also significant, as confirmed by the presence of *Alcaligenes* and *Acinetobacter* in all stages (Hu and Kung, 2000). Organisms reported with gen machinery for dissimilatory nitrate/nitrite reduction to ammonium under anoxic conditions, such as *Lacunisphaera* and *Anaerolinea* (Pan et al., 2020), were also detected at low concentrations

(0.1-0.5%) in S-I and S-II, which might explain the eventual increases in NH_4-N concentration in *Ax* during these stages.

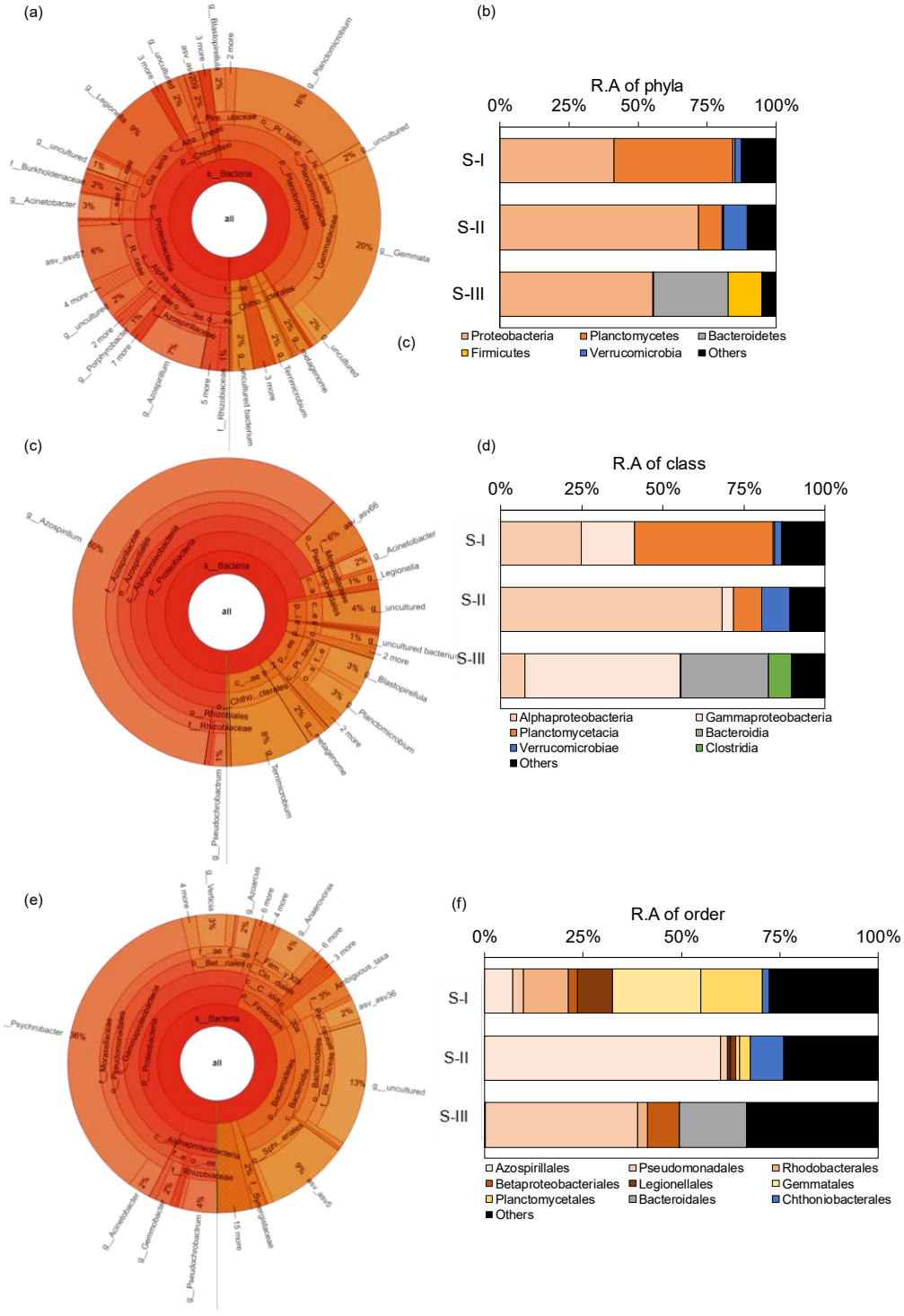

Figure 7 (a) Krona graph and (b) relative abundances (R.A), showing the population structure identified by Illumina at the level of phyla in Stage I, II and III. (c) Krona graph and (d) relative abundances at the level of class and (e) Krona graph and (f) relative abundances at the level of order.

3.6 Microalgae biomass valorization

Under steady-state operation, microalgal-bacterial biomass productivity accounted for 11±3, 15±4, and 9±5 $gVSS \cdot m^{-2} \cdot d^{-1}$ (estimated on the basis of the illuminated area in *OPBR)*. Despite the high operational HRT and SRT herein implemented, these biomass productivities were comparable to those reported in full-scale conventional high rate algal ponds (Fallowfield et al., 2018). Average C, N, P and S contents of 42.1±0.4%, 7.3±0.1%, 0.2±0.01 and 0.4±0.1%, respectively, were recovered in the harvested biomass regardless of the SFWD loading rate. This elemental composition remained within the typical range of values reported in previous works (Marín et al., 2018) and confirms the potential of this microalgal-bacterial biomass for agricultural applications as biofertiliser, thus contributing to closed-cycle management of food waste and similar wastes that can be anaerobically digested, coupling the treatment of the liquid-fraction of digestate to nutrients recovery (Monfet et al., 2017). The direct application of the microalgal-bacterial biomass in soils as fertilizer or bioestimulant (Barone et al., 2018) is a straightforward alternative, mainly in peri-urban areas with favorable climatic conditions, where anaerobic treatment of food wastes can be coupled to microalgae-based treatment of the digestate, with lower transportation costs of both raw waste and the produced biomass.

4 Conclusions

The anoxic-aerobic microalgal-bacterial system herein assessed was confirmed as an efficient and sustainable alternative for the treatment of food waste digestate. High removal efficiencies were achieved for TOC and TN, even when treating undiluted SFWD. O_2 limitation in the photobioreactor during undiluted SFWD treatment inhibited nitrification and decrease phosphorous removal. No external CO_2 supplementation was required to prevent competition

572 between microalgae and nitrifiers, which were simultaneously supported by the high inorganic
573 carbon and nitrogen concentration of the SFWD, temperature and SRT of operation during the
574 treatment of diluted digestate (S-I and S-II). *Chlorella vulgaris* and *Cryptomonas* sp. dominated
575 the microalgal community in S-I and S-II, whereas *Pseudoanabaena* sp. was dominant during S-
576 III. Illumina sequencing revealed the presence of carbon and nitrogen transforming bacteria, whilst
577 *Gemmata*, *Azospirillum* and *Psychrobacter* dominating the bacterial community during S-I, S-II
578 and S-III, respectively. The productivities and elemental composition of the microalgal-bacterial
579 biomass generated suggest that this biomass can be valorised in agricultural applications, thus
580 closing the food waste cycles.

581 **Acknowledgments**

582 This work was supported by the Regional Government of Castilla y León and the EU-FEDER
583 (CLU 2017 – 09 and UIC 071). Authors also acknowledge CNPq for the scholarship 141428/2016-
584 3, and the National Inst. of Sci.&Tech. on Sustainable Sewage Treatment Plants (INCT Sustainable
585 Sewage Treatment Plants) for the mobility grant.

586 **References**

[1] Alcántara, C., Domínguez, J., García, D., Blanco, S., Pérez, R., García-Encina, P., Muñoz, R., 2015a. Evaluation of wastewater treatment in a novel anoxic–aerobic algal–bacterial photobioreactor with biomass recycling through carbon and nitrogen mass balances. Bioresour. Technol. 191, 173-186. doi:10.1016/j.biortech.2015.04.125

[2] Alcántara, C., Muñoz, R., Norvill, Z., Plouviez, M., Guieysse, B., 2015b. Nitrous oxide emissions from high rate algal ponds treating domestic wastewater. Bioresour. Technol. 177, 110-117. doi:10.1016/j.biortech.2014.10.134

[3] Ali, A. A. A., Naddeo, V., Hasan, S., Yousef, A., 2020. Correlation between bacterial community structure and performance efficiency of a full-scale wastewater treatment plant. J. Water Process Eng. 37, 101472. doi:10.1016/j.jwpe.2020.101472

[4] Barone, V., Puglisi, I., Fragalà, F., Stevanato, P., & Baglieri, A. (2019). Effect of living cells of microalgae or their extracts on soil enzyme activities. Arch. Agron. Soil Sci., *65*(5), 712-726. doi.org/10.1080/03650340.2018.1521513

[5] Bernet, N., Habouzit, F., Moletta, R., 1996. Use of an industrial effluent as a carbon source for denitrification of a high-strength wastewater. Appl. Microbiol. Biotechnol. 46, 92-97. doi:10.1007/s002530050788

[6] Boelee, N., Temmink, H., Janssen, M., Buisman, C., Wijffels, R., 2011. Nitrogen and phosphorus removal from municipal wastewater effluent using microalgal biofilms. Water Res. 45, 5925-5933. doi:10.1016/j.watres.2011.08.044

[7] Cai, T., Park, S., Li, Y., 2013. Nutrient recovery from wastewater streams by microalgae: Status and prospects. Renew. Sust. Energ. Rev. 19, 360-369. doi:10.1016/j.rser.2012.11.030

[8] Caicedo, C., Rosenwinkel, K., Exner, M., Verstraete, W., Suchenwirth, R., Hartemann, P., Nogueira, R., 2019. *Legionella* occurrence in municipal and industrial wastewater treatment plants and risks of reclaimed wastewater reuse: Review. Water Res. 149, 21-34. doi:10.1016/j.watres.2018.10.080

[9] Chen, L., Huang, J., Hua, B., Droste, R., Ali, S., Zhao, W., 2020. Effect of steel slag in recycling waste activated sludge to produce anaerobic granular sludge. Chemosphere 257, 127291. doi:10.1016/j.chemosphere.2020.127291

[10] Chouari, R., Le Paslier, D., Daegelen, P., Ginestet, P., Weissenbach, J., Sghir, A., 2003. Molecular Evidence for Novel *Planctomycete* Diversity in a Municipal Wastewater Treatment Plant. Appl. Environ. Microbiol. 69, 7354-7363. doi:10.1128/aem.69.12.7354-7363.2003

[11] Chuka-ogwude, D., Ogbonna, J., Moheimani, N., 2020. A review on microalgal culture to treat anaerobic digestate food waste effluent. Algal Res. 47, 101841. doi:10.1016/j.algal.2020.101841

[12] Collos, Y., Harrison, P., 2014. Acclimation and toxicity of high ammonium concentrations to unicellular algae. Mar. Pollut. Bull. 80, 8-23. doi:10.1016/j.marpolbul.2014.01.006

[13] de Godos, I., Vargas, V., Guzmán, H., Soto, R., García, B., García, P., Muñoz, R., 2014. Assessing carbon and nitrogen removal in a novel anoxic–aerobic cyanobacterial–bacterial photobioreactor configuration with enhanced biomass sedimentation. Water Res. 61, 77-85. doi:10.1016/j.watres.2014.04.050

[14] de-Bashan, L., 2002. Removal of ammonium and phosphorus ions from synthetic wastewater by the microalgae *Chlorella vulgaris* coimmobilized in alginate beads with the microalgae growth-promoting bacterium *Azospirillum brasilense*. Water Res. 36, 2941-2948. doi:10.1016/s0043-1354(01)00522-x

[15] Dhaouefi, Z., Toledo-Cervantes, A., García, D., Bedoui, A., Ghedira, K., Chekir-Ghedira, L., Muñoz, R., 2018. Assessing textile wastewater treatment in an anoxic-aerobic photobioreactor and the potential of the treated water for irrigation. Algal Res. 29, 170-178. doi:10.1016/j.algal.2017.11.032

[16] Elefsiniotis, P., Wareham, D., Smith, M., 2004. Use of volatile fatty acids from an acid-phase digester for denitrification. J. Biotechnol. 114, 289-297. doi:10.1016/j.jbiotec.2004.02.016

[17] Fallowfield, H. J., Young, P., Taylor, M. J., Buchanan, N., Cromar, N., Keegan, A., & Monis, P., 2018. Independent validation and regulatory agency approval for high rate algal ponds

to treat wastewater from rural communities. Environ. Sci.-Water Res., 4(2), 195-205. 10.1039/C7EW00228A

[18] Feng, L., Chen, K., Han, D., Zhao, J., Lu, Y., Yang, G., Mu, J., Zhao, X., 2017. Comparison of nitrogen removal and microbial properties in solid-phase denitrification systems for water purification with various pretreated lignocellulosic carriers. Bioresour. Technol 224, 236-245. doi:10.1016/j.biortech.2016.11.002

[19] Feng, L., Yang, J., Yu, H., Lan, Z., Ye, X., Yang, G., Yang, Q., Zhou, J., 2020. Response of denitrifying community, denitrification genes and antibiotic resistance genes to oxytetracycline stress in polycaprolactone supported solid-phase denitrification reactor. Bioresour. Technol. 308, 123274. doi:10.1016/j.biortech.2020.123274

[20] Frutos, O. D., Quijano, G., Perez, R., & Munoz, R. (2016). Simultaneous biological nitrous oxide abatement and wastewater treatment in a denitrifying off-gas bioscrubber. Chem. Eng. J. 288, 28-37.

[21] Galès, A., Bonnafous, A., Carré, C., Jauzein, V., Lanouguère, E., Le Floc'h, E., Pinoit, J., Poullain, C., Roques, C., Sialve, B., Simier, M., Steyer, J., Fouilland, E., 2019. Importance of ecological interactions during wastewater treatment using High Rate Algal Ponds under different temperate climates. Algal Res. 40, 101508. doi:10.1016/j.algal.2019.101508

[22] García, D., Alcántara, C., Blanco, S., Pérez, R., Bolado, S., Muñoz, R., 2017a. Enhanced carbon, nitrogen and phosphorus removal from domestic wastewater in a novel anoxic-aerobic photobioreactor coupled with biogas upgrading. Chem. Eng. J. 313, 424-434. doi:10.1016/j.cej.2016.12.054

[23] García, D., Posadas, E., Grajeda, C., Blanco, S., Martínez-Páramo, S., Acién, G., García-Encina, P., Bolado, S., Muñoz, R., 2017b. Comparative evaluation of piggery wastewater

treatment in algal-bacterial photobioreactors under indoor and outdoor conditions. Bioresour. Technol. 245, 483-490. doi:10.1016/j.biortech.2017.08.135

[24] González-Camejo, J., Montero, P., Aparicio, S., Ruano, M. V., Borrás, L., Seco, A., & Barat, R. (2020). Nitrite inhibition of microalgae induced by the competition between microalgae and nitrifying bacteria. Wat Res, *172*, 115499.

[25] González-Fernández, C., Molinuevo-Salces, B., García-González, M., 2011. Nitrogen transformations under different conditions in open ponds by means of microalgae–bacteria consortium treating pig slurry. Bioresour. Technol. 102, 960-966. doi:10.1016/j.biortech.2010.09.052

[26] Gutiérrez, J., Kwan, T., Zimmerman, J., Peccia, J., 2016. Ammonia inhibition in oleaginous microalgae. Algal Res 19, 123-127. doi:10.1016/j.algal.2016.07.016

[27] How, S., Chua, A., Ngoh, G., Nittami, T., Curtis, T., 2019. Enhanced nitrogen removal in an anoxic-oxic-anoxic process treating low COD/N tropical wastewater: Low-dissolved oxygen nitrification and utilization of slowly-biodegradable COD for denitrification. Sci. Total Environ. 693, 133526. doi:10.1016/j.scitotenv.2019.07.332

[28] Hu, T., Kung, K., 2000. Study of heterotrophic nitrifying bacteria from wastewater treatment systems treating acrylonitrile, butadiene and styrene resin wastewater. Water Sci. Technol. 42, 315-321. doi:10.2166/wst.2000.0397

[29] Ibekwe, A. M., Murinda, S., Murry, M., Schwartz, G., Lundquist, T., 2017. Microbial community structures in high rate algae ponds for bioconversion of agricultural wastes from livestock industry for feed production. Sci. Total Environ. 580, 1185-1196. doi:10.1016/j.scitotenv.2016.12.076

[30] Kellogg, C., Ross, S., Brooke, S., 2016. Bacterial community diversity of the deep-sea octocoral *Paramuricea placomus*. PeerJ 4, e2529. doi:10.7717/peerj.2529

[31] Klindworth, A., Pruesse, E., Schweer, T., Peplies, J., Quast, C., Horn, M., Glöckner, F., 2012. Evaluation of general 16S ribosomal RNA gene PCR primers for classical and next-generation sequencing-based diversity studies. Nucleic Acids Res. 41, e1-e1. doi:10.1093/nar/gks808

[32] Kundu, P., Pramanik, A., Dasgupta, A., Mukherjee, S., Mukherjee, J., 2014. Simultaneous Heterotrophic Nitrification and Aerobic Denitrification by *Chryseobacterium sp*. R31 Isolated from Abattoir Wastewater. BioMed Research International 2014, 1-12. doi:10.1155/2014/436056

[33] Lee, J., Kim, E., Han, G., Tongco, J., Shin, S., Hwang, S., 2018. Microbial communities underpinning mesophilic anaerobic digesters treating food wastewater or sewage sludge: A full-scale study. Bioresour. Technol. 259, 388-397. doi:10.1016/j.biortech.2018.03.052

[34] Liu, X., Li, H., 2019. Nitrogen removal performance and microorganism community of an A/O-MBBR system under extreme hydraulic retention time. Desalin. Water Treat. 158, 105-113. doi:10.5004/dwt.2019.24268

[35] Makádi, M., Tomócsik, A., Orosz, V., 2010. Digestate: a new nutrient source–review. Biogas 295, 312. DOI: 10.5772/31355

[36] Marín, D., Posadas, E., Cano, P., Pérez, V., Blanco, S., Lebrero, R., Muñoz, R., 2018. Seasonal variation of biogas upgrading coupled with digestate treatment in an outdoors pilot scale algal-bacterial photobioreactor. Bioresour. Technol. 263, 58-66. doi:10.1016/j.biortech.2018.04.117

[37] Monfet, E., Aubry, G., & Ramirez, A. A. (2018). Nutrient removal and recovery from digestate: a review of the technology. Biofuels, *9*(2), 247-262.

[38] Ondov, B., Bergman, N., Phillippy, A., 2011. Interactive metagenomic visualization in a Web browser. BMC Bioinformatics 12. doi:10.1186/1471-2105-12-385

[39] Pan, H., Yuan, D., Liu, W., Pi, Y., Wang, S., Zhu, G., 2020. Biogeographical distribution of dissimilatory nitrate reduction to ammonium (DNRA) bacteria in wetland ecosystems around the world. J. Soils Sediments. 20(10), 3769-3778. doi:10.1007/s11368-020-02707-y

[40] Pascual, C., Akmirza, I., Pérez, R., Arnaiz, E., Muñoz, R., Lebrero, R., 2020. Trimethylamine abatement in algal-bacterial photobioreactors. Environ. Sci. Pollut. Res. 27, 9028-9037. doi:10.1007/s11356-019-07369-z

[41] Rada-Ariza, A., Lopez-Vazquez, C., van der Steen, N., Lens, P., 2017. Nitrification by microalgal-bacterial consortia for ammonium removal in flat panel sequencing batch photo-bioreactors. Bioresour. Technol. 245, 81-89. doi:10.1016/j.biortech.2017.08.019

[42] Rahman, A., De Clippeleir, H., Thomas, W., Jimenez, J., Wett, B., Al-Omari, A., Murthy, S., Riffat, R., Bott, C., 2019. A-stage and high-rate contact-stabilization performance comparison for carbon and nutrient redirection from high-strength municipal wastewater. Chem. Eng. J. 357, 737-749. doi:10.1016/j.cej.2018.09.206

[43] Rehl, T., Müller, J., 2011. Life cycle assessment of biogas digestate processing technologies. Resour. Conserv. Recy. 56, 92-104. doi:10.1016/j.resconrec.2011.08.007

[44] Risgaard-Petersen, N., Nicolaisen, M., Revsbech, N., Lomstein, B., 2004. Competition between Ammonia-Oxidizing Bacteria and Benthic Microalgae. Appl. Environ. Microb. 70, 5528-5537. doi:10.1128/aem.70.9.5528-5537.2004

[45] Schmieder, R., Edwards, R., 2011. Quality control and preprocessing of metagenomic datasets. Bioinformatics 27, 863-864. doi:10.1093/bioinformatics/btr026

[46] Shoda, M., Ishikawa, Y., 2014. Heterotrophic nitrification and aerobic denitrification of high-strength ammonium in anaerobically digested sludge by *Alcaligenes faecalis* strain No. 4. J. Biosci. Bioeng. 117, 737-741. doi:10.1016/j.jbiosc.2013.11.018

[47] Si, Z., Peng, Y., Yang, A., Zhang, S., Li, B., Wang, B., Wang, S., 2018. Rapid nitrite production via partial denitrification: pilot-scale operation and microbial community analysis. Environmental Science: Water Research & Technology 4, 80-86. doi:10.1039/c7ew00252a

[48] Solovchenko, A., Verschoor, A., Jablonowski, N., Nedbal, L., 2016. Phosphorus from wastewater to crops: An alternative path involving microalgae. Biotechnol. Adv. 34, 550-564. doi:10.1016/j.biotechadv.2016.01.002

[49] Sournia A., Phytoplankton Manual, UNESCO, Paris, 1978, <http://unesdoc. unesco.org/images/0003/000307/030788eo.pdf>.

[50] Stiles, W., Styles, D., Chapman, S., Esteves, S., Bywater, A., Melville, L., Silkina, A., Lupatsch, I., Fuentes Grünewald, C., Lovitt, R., Chaloner, T., Bull, A., Morris, C., Llewellyn, C., 2018. Using microalgae in the circular economy to valorise anaerobic digestate: challenges and opportunities. Bioresour. Technol. 267, 732-742. doi:10.1016/j.biortech.2018.07.100

[51] Toledo-Cervantes, A., Posadas, E., Bertol, I., Turiel, S., Alcoceba, A., & Muñoz, R. (2019). Assessing the influence of the hydraulic retention time and carbon/nitrogen ratio on urban wastewater treatment in a new anoxic-aerobic algal-bacterial photobioreactor configuration. Algal Res. 44, 101672.

[52] Wett, B., Rauch, W., 2003. The role of inorganic carbon limitation in biological nitrogen removal of extremely ammonia concentrated wastewater. Water Res. 37, 1100-1110. doi:10.1016/s0043-1354(02)00440-2

[53] White, D., Pagarette, A., Rooks, P., Ali, S., 2012. The effect of sodium bicarbonate supplementation on growth and biochemical composition of marine microalgae cultures. J. Appl. Phycol. 25, 153-165. doi:10.1007/s10811-012-9849-6

[54] Xia, Z., Wang, Q., She, Z., Gao, M., Zhao, Y., Guo, L., Jin, C., 2019. Nitrogen removal pathway and dynamics of microbial community with the increase of salinity in simultaneous

nitrification and denitrification process. Sci. Total Environ. 697, 134047. doi:10.1016/j.scitotenv.2019.134047

[55] Yi, J., Dong, B., Jin, J., Dai, X., 2014. Effect of Increasing Total Solids Contents on Anaerobic Digestion of Food Waste under Mesophilic Conditions: Performance and Microbial Characteristics Analysis. PLoS ONE 9, e102548. doi:10.1371/journal.pone.0102548

[56] Yuan, M., Chen, Y., Tsai, J., Chang, C., 2016. Ammonia removal from ammonia-rich wastewater by air stripping using a rotating packed bed. Process Saf. Environ. 102, 777-785. doi:10.1016/j.psep.2016.06.021

587

588 **Supplementary Data**

589 **ASSESSMENT OF THE PERFORMANCE OF AN ANOXIC-AEROBIC**

590 **MICROALGAL-BACTERIAL SYSTEM TREATING DIGESTATE**

591 Andrés F. Torres-Franco [a, b, c], Maribel Zuluaga [a, b, d], Diana Hernández-Roldán [a, b, d], Deborah

592 Leroy-Freitas [a, b, c], Cristian A. Sepúlveda-Muñoz [a, b], Saúl Blanco [e, f], César R. Mota [c], Raúl

593 Muñoz [a, b, *]

594 [a] Department of Chemical Engineering and Environmental Technology, Valladolid University,
595 Dr. Mergelina, s/n., 47011 Valladolid, Spain.

596 [b] Institute of Sustainable Processes, Dr. Mergelina, s/n, 47011, Valladolid, Spain.

597 [c] Department of Sanitary and Environmental Engineering, Federal University of Minas Gerais,
598 Belo Horizonte, 31270-010, Brazil.

599 [d] Faculty of Environmental Engineering UPAEP University, Puebla, 21 Sur 1103, Barrio de
600 Santiago, 72410, Puebla, México.

601 [e] University of León, Campus de Vegazana, 24071, León, Spain.

602 [f] Laboratory of Diatomology. Institute of Environment, Natural Resources and Biodiversity. La
603 Serna 58, 24007, León, Spain

604 * Corresponding author: mutora@iq.uva.es, *Tel*: (34) 983-186-424 (R. Muñoz)

605 **Table S1**

606 **Figure S1**

607 **Figure S2**

608 **Table S1.** Contribution of the different mechanisms involved in nitrogen transformation in the
609 anoxic-aerobic system
610

Stage	% influent TN			
	Effluent	**Stripping**	**Denitrification**	**Biomass uptake**
I	16 ± 3	23 ± 15	32 ± 13	30 ± 7
II	21 ± 6	33 ± 20	31 ± 33	15 ± 4
III	27 ± 3	68 ± 4	0 ± 1	5 ± 2

611

612 **Figure S1**

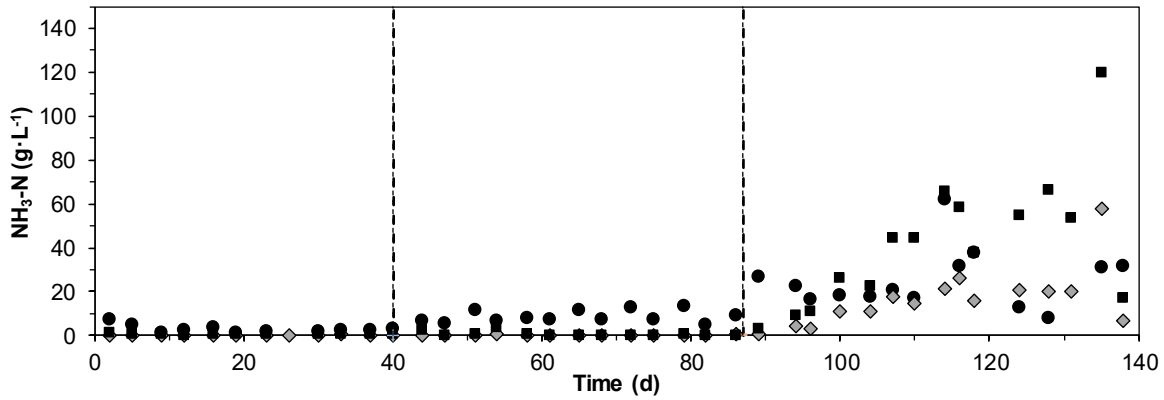

613 **Figure S1.** Time course of NH_3-N estimated for (●) influent SFWD, (▲) *Ax*, (■) *OPBR* and (◆) final
614 effluent (*E*).
615

Figure S2

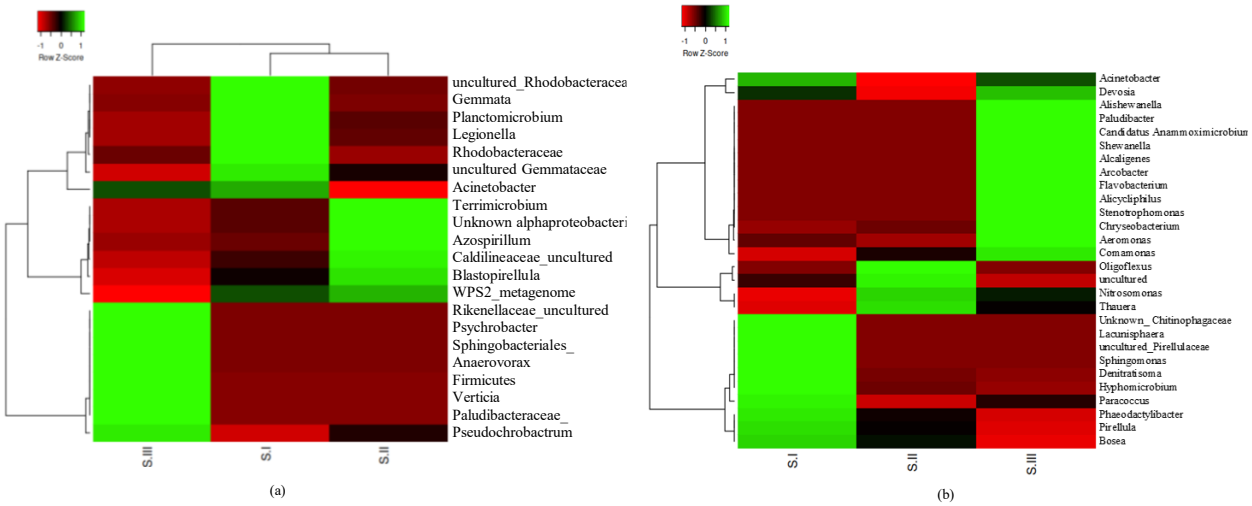

Figure S2 (a) Heatmap for main genera accumulating 90% of the total abundance and (b) Heatmap for the main bacteria related to nitrogen removal processes. Heatmaps elaborated with Heatmapper: web-enabled heat mapping for all. *Nucleic Acids Res.* 2016 May 17 (epub ahead of print). doi:10.1093/nar/gkw419